Geophys. Astrophys. Fluid Dynamics, Vol. 45, pp. 37–69
Reprints available directly from the publisher
Photocopying permitted by license only

TIDE-TOPOGRAPHY INTERACTIONS IN A STRATIFIED SHELF SEA II. BOTTOM TRAPPED INTERNAL TIDES AND BAROCLINIC RESIDUAL CURRENTS

L. R. M. MAAS* and J. T. F. ZIMMERMAN*†

**Netherlands Institute for Sea Research, P.O. Box 59, 1970 AB Den Burg, Texel, The Netherlands*
†Institute of Meteorology and Oceanography, Buys Ballot Laboratory, University of Utrecht, The Netherlands

(Received 22 February 1988; in final form 22 June 1988)

The generation of topographically bounded internal tides and baroclinic residual currents is discussed for a linearly stratified fluid in the limit of small-amplitude topography and weak damping. It is shown that quasi-nonlinear advection by the barotropic tide generates a residual and higher harmonics, besides the ever present fundamental driving frequency in the internal motions. At all frequencies the along-isobath currents and the cross-isobath circulation are *bottom intensified*, the intensification being a function of the internal Rossby deformation radius. For a step topography the weak cross-isobath residual circulation has a characteristic three-cell structure with a down-slope bottom current at the position of the steepest slope, which is also the center of the along-isobath residual jet. In contrast to barotropic currents in the quasi-nonlinear regime, the baroclinic currents are exponentially bounded to the topography, rather than extending over a finite interval, in which the *e*-folding distance is the internal deformation radius.

KEY WORDS: Tide-topography interaction; bottom intensification; internal tides; baroclinic residual current; stratified shelf sea; quasi-nonlinear advection; geostrophic adjustment; vortex stretching.

1. INTRODUCTION

In the preceding paper (Maas and Zimmerman, 1988; henceforth referred to as I) it was shown that the free modes of a dissipative, stratified, uniformly rotating fluid consist of damped propagating gravity waves and a non-propagating transient. The latter is usually neglected, but in problems of a localized forcing, these transients can give rise to a spatially bounded response; i.e. in the present context to topographically trapped modes. These are the subject of this second part, whereas the gravity waves are dealt with in Maas and Zimmerman (1989), henceforth referred to as III.

The importance of a nonpropagating transient is well-known in the barotropic theory of tide-topography interactions, where its presence gives rise to nonlinear generation of residual currents and overtides (Huthnance, 1973; Zimmerman, 1978, 1980; Loder, 1980). One could expect such phenomena to occur in a stratified fluid as well, but to our knowledge there exists no theory of baroclinic topographic

rectification and the associated topographically bounded overtides. For tidally rectified currents the presence of stratification has only been dealt with in a passive way by means of its influence on vertical momentum exchange (Loder and Wright, 1985; Tee, 1985), which in turn influences the vertical structure of residual currents. Frictionally-induced vertical structure of residual circulation has been given much attention recently (Wright and Loder, 1985; Tee, 1985; Ou and Maas, 1986; Yasuda and Zimmerman, 1986). The presence of Ekman-Stokes layers near the bottom gives rise to vertical shear of the along-isobath velocity and to an often complicated cross-isobath circulation. One of our purposes here is to show that these features also occur due to baroclinicity. However, instead of the usual increase in strength of a current from the bottom upwards in the presence of friction, we find that one of the main properties of along and cross-isobath baroclinic residual circulation is bottom-trapping. This also applies to the topographically bounded internal tides and overtides. We are able to separate the influence of baroclinicity on the vertical structure from that of (bottom) friction, as we are dealing with parametrized damping of individual vertical modes, as discussed in I. The response of an individual vertical mode to a topography with a single horizontal wave number is discussed in Section 2 for a quasi-Lagrangian and a Eulerian frame of reference. The results are used in Section 3 for calculating the spectral response of modal cross-isobath stream function, along-isobath velocity and the pressure distribution (isopycnal elevation field). Summing the vertical modes in Section 4 gives the vertical structure for these dynamic field variables for a linearly stratified fluid, showing the phenomenon of bottom intensification in stratified circumstances and the influence of quasi-nonlinear advection. These results, finally, are used in Section 5 in an inverse Fourier transform for a ridge- and steptopography, which gives the complete vertical structure of baroclinic residual currents and topographically bounded tides and overtides in the neighbourhood of these topographic features.

2. SPECTRAL RESPONSE OF MODAL VERTICAL VELOCITY AMPLITUDES

Our starting point is the equation (I; 5.12) for the forcing of vertical normal modes of the spectral vertical velocity amplitudes for a linearly stratified fluid in a quasi-Lagrangian frame of reference, moving with the basic barotropic tidal current over a one-dimensional, y-independent, topography, with spectral amplitude $\hat{H}(k)$:

$$\left[\frac{\partial^3}{\partial t^3}+2r_n\frac{\partial^2}{\partial t^2}+\left(f^2+r_n^2+\frac{k^2}{k_n^2}\right)\frac{\partial}{\partial t}+r_n\frac{k^2}{k_n^2}\right]\hat{W}_n=\hat{F}_n(k,t), \tag{2.1}$$

where

$$\hat{F}_n(k,t)=a_n(k)e^{ik\sin t}\left(\frac{\partial}{\partial t}+ik\cos t+r_n\right)\cos t, \tag{2.2}$$

with

$$a_n(k)=\frac{2}{n^2\pi^2}\frac{k^2}{k_n^2}ik\hat{H}(k)=2c_n^2ik\hat{H}(k)\frac{k^2}{k_n^2}. \tag{2.3}$$

Variables in (2.1)–(2.3) are non-dimensional, scaled according to the scheme given in (I; 2.3) except for the topographic wavenumber, k, which is, as discussed in (I; 5), rescaled with the tidal excursion amplitude, $l_0=U/\sigma$, where U is the amplitude of the cross-isobath component of the barotropic tidal current and σ its frequency. That is, $k=k_*l_0$ where k_* is the dimensional wavenumber, while the "fast" coordinate over which the topography varies is rescaled simultaneously, i.e. $x=x_*/l_0$. As both l_0 and the internal wave length scale, $l_i=N_*H_0/\sigma$ (with N_* the constant Brunt-Väisäla frequency and H_0 the mean depth) are of the same order this does not affect the multiple scale analysis in (I; 2), but it makes possible a more transparent comparison of the results given here with those of a purely barotropic situation.

The remaining dimensionless parameters in (2.1)–(2.3) are: the modal damping coefficient,

$$r_n=E_-^{1/2}+\tfrac{1}{2}E_-n^2\pi^2, \tag{2.4}$$

dominated by the Ekman-Stokes number due to the anticyclonically rotating current component:

$$E_-=\frac{E_s}{1-f}=\frac{2K}{\sigma H_0^2(1-f)}, \tag{2.5}$$

f, being the dimensional Coriolis frequency f_* scaled by the tidal frequency σ and K a constant vertical eddy viscosity. Moreover

$$k_n=n\pi l_0/l_i. \tag{2.6}$$

The quasi-Lagrangian modal amplitude of the vertical velocity, $\hat{W}_n(k,t)$, is related to its Eulerian counterpart, $\hat{w}_n(k,t)$, by

$$\hat{w}_n(k,t)=\hat{W}_n(k,t)\exp\left[-i\int^t ku^{(0)}(t')dt'\right]=\hat{W}_n\exp(ik\sin t), \tag{2.7}$$

using $u^{(0)}(t)=\cos t$ for the cross-isobath barotropic velocity component.

The homogeneous part of (2.1) is satisfied by

$$\hat{W}_n=\sum_{i=1}^{3}A_i\,e^{\nu_i t}, \tag{2.8}$$

with unspecified amplitudes A_i. The three characteristic roots, ν_i, have been discussed extensively in (I; Sect. 6), where explicit expressions for several limiting

situations are given, from which we quote the results for weak damping, which we shall also use later:

$$\nu_{1,2} = \nu_R \pm i\nu_I,$$

$$\nu_R = -r_n \frac{(k^2/k_n^2 + 2f^2)}{2(k^2/k_n^2 + f^2)}, \tag{2.9a}$$

$$\nu_I = \left(f^2 + \frac{k^2}{k_n^2}\right)^{1/2}, \tag{2.9b}$$

$$\nu_3 = -r_n \frac{k^2/k_n^2}{f^2 + k^2/k_n^2}. \tag{2.9c}$$

In combination with the forcing as described in the right-hand side of (2.1) each of these roots gives rise to a response. For the complex roots, $\nu_{1,2}$, this response is in the form of damped propagating gravity waves that are the subject of III. Here we shall be concerned with the third root, ν_3, describing a transient that, in combination with the forcing, gives rise to topographically bounded nontransient effects, for which the forced response reads:

$$\hat{W}_n(k,t) = \frac{e^{\nu_3 t} \int_{-\infty}^{t} e_{t'}^{-\nu_3 t'} \hat{F}_n(k,t')\, dt'}{\nu_I^2 + (\nu_R - \nu_3)^2}. \tag{2.10}$$

We write the forcing in the right-hand side of (2.1) as

$$\hat{F}_n(k,t) = a_n(k) e^{ik \sin t} \sum_{q=-2}^{2} C_q\, e^{iqt} \tag{2.11}$$

where

$$C_0 = \frac{ik}{2}, \quad C_{\pm 1} = \frac{r_n \pm i}{2}, \quad C_2 = C_{-2} = \frac{ik}{4}, \tag{2.12}$$

and adopt the expansion of $\exp(ik \sin t)$ in terms of Bessel functions

$$e^{ik \sin t} = \sum_{m=-\infty}^{\infty} J_m(k) e^{imt}. \tag{2.13}$$

Then

$$e^{\nu_3 t} \sum_{m} \sum_{q=-2}^{2} \int_{-\infty}^{t} C_q J_m(k) e^{(im - \nu_3 + iq)t'} dt' = \sum_{m} \sum_{q=-2}^{2} C_q J_m(k) \frac{1}{i(m+q) - \nu_3} e^{i(m+q)t}. \tag{2.14}$$

With a shift of indices, (2.14) is equal to

$$\sum_m \frac{1}{im-\nu_3}\left\{\sum_{q=-2}^{2}[C_q J_{m-q}(k)]\right\}e^{imt}. \tag{2.15}$$

With the expressions for the C_q (2.12) and the addition and subtraction rules for the Bessel functions (Appendix, Eq. (A1)) we evaluate

$$\sum_{q=-2}^{2} C_q J_{m-q}(k) = (r_n + im)mJ_m(k)/k. \tag{2.16}$$

Substitution of this result in (2.10) finally gives

$$\hat{W}_n(k,t) = \frac{a_n(k)}{k}\sum_m \frac{(r_n+im)m\,J_m(k)e^{imt}}{\{\nu_I^2+(\nu_R-\nu_3)^2\}\{im-\nu_3\}}. \tag{2.17}$$

The quasi-Lagrangian solution shows that a single forcing frequency ($m=1$) in the barotropic current generates all harmonics, $m \geqslant 1$, in the internal modes but, for a small-amplitude topography to this order in the perturbation theory, no Lagrangian baroclinic residual current ($m=0$).

The solution in the Eulerian frame, using (2.7) and (2.13) reads from (2.17):

$$\hat{w}_n(k,t) = \sum_{q=-\infty}^{\infty} C_{qn}(k)e^{-iqt}, \tag{2.18}$$

where

$$C_{qn}(k) = \frac{a_n}{k}\sum_m \frac{(r_n+im)mJ_m(k)J_{m+q}(k)}{\{\nu_I^2+(\nu_R-\nu_3)^2\}\{im-\nu_3\}}. \tag{2.19}$$

Thus, also in the Eulerian solution, besides the basic frequency, $q=\pm 1$, all superharmonics are present, as well as a Eulerian residual effect, $q=0$. This is the same behaviour as found for barotropic residual circulation (Maas *et al.*, 1987) where, for the residual circulation related to stretching of planetary vorticity (the "Coriolis effect"), the quasi-Lagrangian result vanishes, whereas the Eulerian does not. Any residual circulation in the quasi-Lagrangian frame is then due to differential bottom friction, a mechanism that is absent for the internal modes in this order of our perturbation theory. This accords with results for barotropic residual circulation for a finite-amplitude topography (Huthnance, 1973; Loder, 1980), when taking the limit of a small topographic amplitude. For finite amplitude though, also the Coriolis-effect gives a nonzero Lagrangian barotropic residual circulation, which one therefore could expect for internal modes too. However, more definitive statements have to wait for an analytical treatment of the finite-amplitude case.

3. SPECTRAL RESPONSE OF MODAL CROSS-ISOBATH STREAM FUNCTION, ALONG-ISOBATH VELOCITY AND ISOPYCNAL ELEVATION

For a topography depending only on x, we can assume that y-derivatives vanish. From (I; 2.45c) we may then define a cross-isobath stream function ψ such that

$$w = \frac{\partial \psi}{\partial x}, \qquad u = -\frac{\partial \psi}{\partial z}, \tag{3.1}$$

describing the circulation in the x–z plane normal to the isobaths. This stream function ψ, together with the along-isobath velocity v and pressure field p (hydrostatically related to the isopycnal displacements, ζ) depicts the total perturbation field due to tide-topography interaction as far as the vorticity wave modes are concerned. The spectral amplitudes of these variables can easily be related to the spectral velocity components $\hat{W}_n$ (obtained in the Lagrangian frame), given by (2.17), through the modal equations (I; 5.2). By returning to the Eulerian frame, with the aid of (2.7), we find:

$$\hat{\phi}_n = \sum_{q=-\infty}^{\infty} \sum_{m=-\infty}^{\infty} \tilde{\phi}_m J_m(k) J_{m+q}(k) e^{-iqt}. \tag{3.2}$$

Here ϕ denotes each of the dynamic variables ψ, v and p. The "amplitudes" $\tilde{\phi}_m$ contain k and n dependent constants:

$$\begin{Bmatrix} \tilde{\psi}_m \\ \tilde{v}_m \\ \tilde{p}_m \end{Bmatrix} = -\frac{a_n}{k^2} \quad \frac{1}{v_I^2 + (v_R - v_3)^2} \quad \frac{m}{im - v_3} \quad \begin{Bmatrix} -m + ir_n \\ if/c_n^2 \\ \dfrac{1}{c_n^2 k}(f^2 + (im + r_n)^2) \end{Bmatrix}.$$

In this paper we will give particular consideration to the most dominant frequencies; i.e. the residual ($q=0$), the fundamental harmonic ($q=1$) and the second harmonic ($q=2$). Application of the addition and subtraction rules of the Bessel functions as given in (A1) allows (3.2) to be rewritten in terms of Bessel functions of order m only:

$$\left.\begin{aligned}
&\hat{\phi}_n = \sum_m \tilde{\phi}_m J_m^2, && \text{if } q=0,\\
&\hat{\phi}_n = \sum_m \tilde{\phi}_m \left[\frac{2mJ_m^2}{k} \cos t + i \frac{dJ_m^2}{dk} \sin t \right], && \text{if } q=1,\\
&\hat{\phi}_n = \sum_m \tilde{\phi}_m \left[2\left\{ \left(\frac{2m^2}{k^2} - 1 \right) J_m^2 - \frac{1}{k} \frac{dJ_m^2}{dk} \right\} \cos 2t + \right.\\
&\qquad\qquad \left. + i \frac{2m}{k} \left\{ \frac{dJ_m^2}{dk} - \frac{2J_m^2}{k} \right\} \sin 2t \right], && \text{if } q=2.
\end{aligned}\right\} \tag{3.4}$$

The symmetry property ($A_{-n} = -A_n$) of the squared Bessel functions for odd functions A_n,

$$\sum_{n=-\infty}^{\infty} A_n J_n^2(k) = 0, \tag{3.5}$$

can be used to reduce the expressions, after substitution of the amplitudes $\tilde{\phi}_m$ from (3.3). Here we shall especially consider the limit of weak damping $r_n \to 0$, as this allows us to perform the summations over m analytically [see (A2)]. Since by (2.9) $\nu_3 \sim r_n$, the limit $r_n \to 0$ also allows, up to $O(r_n)$, the interchange of differentiation to k and summations over m:

$$\sum_m \frac{1}{m^2 + \nu_3^2} \frac{d}{dk}(\cdots). \tag{3.6}$$

Hence we find by substitution of (A2), using the amplitudes (3.3) in (3.4) and using (2.9) to eliminate $1/[\nu_I^2 + (\nu_R - \nu_3)^2]$, to lowest order in r_n, for frequencies q:

$$q=0 \begin{cases} \hat{\psi}_n = \dfrac{a_n}{k^2} \dfrac{1}{f^2 + k^2/k_n^2} [-(r_n + \nu_3)](1 - J_0^2), \\ \hat{v}_n = \dfrac{a_n}{k^2} \dfrac{1}{f^2 + k^2/k_n^2} \dfrac{f}{c_n^2} [-(1 - J_0^2)], \\ \hat{p}_n = \dfrac{a_n}{k^3} \dfrac{1}{f^2 + k^2/k_n^2} \dfrac{1}{c_n^2} \left\{ -i \left[\dfrac{k^2}{2} - f^2(1 - J_0^2) \right] \right\}, \end{cases} \tag{3.7a}$$

$$q=1 \begin{cases} \hat{\psi}_n = \dfrac{a_n}{k} \left[\dfrac{-i}{f^2 + k^2/k_n^2} \right] \cos t, \\ \hat{v}_n = \dfrac{a_n}{k^2} \left[\dfrac{-i}{f^2 + k^2/k_n^2} \right] \dfrac{f}{c_n^2} 2 J_0 J_1 \sin t, \\ \hat{p}_n = \dfrac{a_n}{k^3} \left[\dfrac{1}{f^2 + k^2/k_n^2} \right] \dfrac{1}{c_n^2} [k - f^2 J_0 J_1] \sin t, \end{cases} \tag{3.7b}$$

$$q=2 \begin{cases} \hat{\psi}_n = \dfrac{a_n}{k^2} \dfrac{1}{f^2 + k^2/k_n^2} (r_n + \nu_3) 2 J_0 J_2 \cos 2t, \\ \hat{v}_n = \dfrac{a_n}{k^2} \dfrac{1}{f^2 + k^2/k_n^2} \left[\dfrac{f}{c_n^2} \right] 2 J_0 J_2 \cos 2t, \\ \hat{p}_n = \dfrac{a_n}{k^3} \dfrac{1}{f^2 + k^2/k_n^2} \left[\dfrac{-i}{c_n^2} \right] \left(\dfrac{k^2}{2} + 2 f^2 J_0 J_2 \right) \cos 2t, \end{cases} \tag{3.7c}$$

where the argument of all Bessel functions, J_n, is k.

These solutions have the following properties:

(1) The residual ($q=0$) and second harmonic ($q=2$) cross-isobath circulations are weak [$O(r_n)$];
(2) The first harmonic pressure and along-isobath velocity oscillation are in quadrature with the zeroth order tidal current ($\propto \cos t$). The cross-isobath circulation however is in phase with it;
(3) For the second harmonic these three fields are in phase with each other;
(4) The spectral amplitudes of the second harmonic are equivalent to those of the residual field except for a difference of Bessel functions that describe the influence of tidal advection;
(5) In the nonrotating case, $f=0$, the along-isobath velocity vanishes in all harmonics, particularly in the residual. Residual circulation in the cross-isobath plane, though dependent on f, does not vanish in that case.

Many of these properties will be discussed in subsequent Sections.

Before now using these vertical modes in assessing the complete vertical structure for a linearly stratified fluid, we introduce the internal Rossby deformation radius

$$l_i' = l_i/f = N_* H_0/f_*, \tag{3.8}$$

in terms of which we define the wavenumber

$$k' = k l_i'/l_0 = k_* l_i'. \tag{3.9}$$

This makes possible to factor out in (3.7) those parts that depend on mode number (n) and stratification (l_i') and those that depend only on the tidal excursion amplitude (l_0). When we substitute

$$r_n + \nu_3 = r_n \frac{f^2}{f^2 + k^2/k_n^2},$$

using (2.9c) and the amplitude a_n, from (2.3), in (3.7) we get:

$$q=0 \begin{cases} \hat{\psi}_n = 2c_n^2 r_n \dfrac{n^2\pi^2 k'^2}{(n^2\pi^2+k'^2)^2}(-ik\hat{H})\left(\dfrac{1-J_0^2(k)}{k^2}\right), \\ \hat{v}_n = 2f \dfrac{k'^2}{n^2\pi^2+k'^2}(-ik\hat{H})\left(\dfrac{1-J_0^2(k)}{k^2}\right), \\ \hat{p}_n = 2\dfrac{k'^2}{n^2\pi^2+k'^2}\hat{H}\left[\dfrac{1}{2} - f^2\left(\dfrac{1-J_0^2(k)}{k^2}\right)\right], \end{cases} \tag{3.10a}$$

$$q=1\begin{cases}\hat{\psi}_n=2c_n^2\dfrac{k'^2}{n^2\pi^2+k'^2}\hat{H}\cos t,\\ \hat{v}_n=2f\dfrac{k'^2}{n^2\pi^2+k'^2}\hat{H}\left(\dfrac{2J_0(k)J_1(k)}{k}\right)\sin t,\\ \hat{p}_n=2i\dfrac{k'^2}{n^2\pi^2+k'^2}\dfrac{\hat{H}}{k}\left[1-f^2\left(\dfrac{2J_0(k)J_1(k)}{k}\right)\right]\sin t,\end{cases} \tag{3.10b}$$

$$q=2\begin{cases}\hat{\psi}_n=2c_n^2r_n\dfrac{n^2\pi^2k'^2}{(n^2\pi^2+k'^2)^2}ik\hat{H}\left(\dfrac{2J_0(k)J_2(k)}{k^2}\right)\cos 2t,\\ \hat{v}_n=2f\dfrac{k'^2}{n^2\pi^2+k'^2}ik\hat{H}\left(\dfrac{2J_0(k)J_2(k)}{k^2}\right)\cos 2t,\\ \hat{p}_n=2\dfrac{k'^2}{n^2\pi^2+k'^2}\hat{H}\left[\dfrac{1}{2}+f^2\left(\dfrac{2J_0(k)J_2(k)}{k^2}\right)\right]\cos 2t.\end{cases} \tag{3.10c}$$

As will become clear in the next section, it are those factors in (3.10) which depend on the internal Rossby deformation radius that govern the vertical structure of the cross-isobath stream function and the along-isobath velocity component.

4. VERTICAL STRUCTURE OF THE SPECTRAL RESPONSE

The vertical structure of the response to a sinusoidal topography can now be obtained by adding all vertical modes, i.e.

$$\begin{Bmatrix}\hat{\psi}(z)\\ \hat{v}(z)\\ \hat{p}(z)\end{Bmatrix}=\sum_n\begin{Bmatrix}\hat{\psi}_n n\pi\sin n\pi(z+1)\\ \hat{v}_n\cos n\pi(z+1)\\ \hat{p}_n\cos n\pi(z+1)\end{Bmatrix}, \tag{4.1}$$

where the eigenfunctions for a linearly stratified fluid have been discussed in Section 3 of I. For the baroclinic field the summation runs from $n=1$ to ∞. Using (A4) this yields, e.g. for the spectral, along-isobath residual ($q=0$) current:

$$\hat{v}(k,z)=-ik\hat{H}f\left[k'\frac{\cosh k'z}{\sinh k'}-1\right]\left(\frac{1-J_0^2(k)}{k^2}\right). \tag{4.2}$$

To this we may add the barotropic along-isobath residual flow. In the limit of weak friction, using only that part of the residual current that is due to planetary vortex

stretching, the barotropic component reads (Zimmerman, 1978, 1980; Maas *et al.*, 1987):

$$\hat{v} = -ik\hat{H}f\left(\frac{1-J_0^2(k)}{k^2}\right). \tag{4.3}$$

Thus the total along-isobath residual current field reads:

$$\hat{v}(k,z) = -ik\hat{H}f\,\frac{k'\cosh k'z}{\sinh k'z}\left(\frac{1-J_0^2(k)}{k^2}\right), \tag{4.4}$$

which in the limit $k' \to 0$ reduces to (4.3).

This limit corresponds to the situation that the external cross-isobath tidal excursion is much larger than the internal Rossby deformation radius l_i', as when the stratification is very weak. Also note that strong stratification ($l_i' \gg l_0$, hence $k' \to \infty$) inhibits the motions higher up from the bottom and yields an intensified, rectified flow near the bottom (with factor l_i'/l_0)

$$\lim_{k' \to \infty} \hat{v} = f(-ik^2\hat{H})\frac{l_i'}{l_0}\,e^{-k'(z+1)}\left(\frac{1-J_0^2(k)}{k^2}\right). \tag{4.5}$$

The cross-isobath stream function is multiplied by $n\pi \sin n\pi(z+1)$. Note that the forced part of the vertical velocity, $w_e^{(0)}$, see (I; 2.45d), is not incorporated in $\hat{\psi}$ to illuminate the free mode circulation. One final remark is needed to perform the summations over the vertical modes. In the limit of weak damping r_n approaches a constant ($E^{1/2}$); see (2.4). For this reason the index n is dropped: r referring to this constant damping term ($r = E^{1/2}$). Carrying out these summations, using (A5) and (A6), we find for the limit of weak damping:

$$q=0\begin{cases} \hat{\psi} = r(-ik\hat{H})\dfrac{k'}{\tanh k'}\left[z\dfrac{\cosh k'z}{\cosh k'} - \dfrac{\sinh k'z}{\sinh k'}\right]\left(\dfrac{1-J_0^2(k)}{k^2}\right), \\ \hat{v} = f(-ik\hat{H})\dfrac{k'}{\sinh k'}\cosh k'z\left(\dfrac{1-J_0^2(k)}{k^2}\right), \\ \hat{p} = \hat{H}\dfrac{k'}{\sinh k'}\cosh k'z\left[\dfrac{1}{2} - f^2\left(\dfrac{1-J_0^2}{k^2}\right)\right], \end{cases} \tag{4.6a}$$

$$q=1\begin{cases} \hat{\psi} = \cos t\hat{H}\left[\dfrac{\sinh k'z}{\sinh k'} - z\right], \\ \hat{v} = \sin tf\hat{H}\,\dfrac{k'}{\sinh k'}\cosh k'z\,\dfrac{2J_0(k)J_1(k)}{k}, \\ \hat{p} = \sin ti\,\dfrac{\hat{H}}{k}\,\dfrac{k'}{\sinh k'}\cosh k'z\left[1 - f^2\,\dfrac{2J_0(k)J_1(k)}{k}\right], \end{cases} \tag{4.6b}$$

$$q=2\begin{cases}\hat{\psi}=\cos t\, r(-ik\hat{H})\dfrac{k'}{\tanh k'}\left[z\dfrac{\cosh k'z}{\cosh k'}-\dfrac{\sinh k'z}{\sinh k'}\right] \\ \qquad\times\left(\dfrac{-2J_0(k)J_2(k)}{k^2}\right), \\ \hat{v}=\cos 2t f(-ik\hat{H})\dfrac{k'}{\sinh k'}\cosh k'z\left(\dfrac{-2J_0(k)J_2(k)}{k^2}\right), \\ \hat{p}=\cos 2t\hat{H}\dfrac{k'}{\sinh k'}\cosh k'z\left[\dfrac{1}{2}+f^2\dfrac{2J_0(k)J_2(k)}{k^2}\right].\end{cases} \tag{4.6c}$$

It is interesting to observe that all functions have a similar form:

$$\hat{\phi}=f(t)T(\hat{H},k)S(k',z)A(k), \tag{4.7}$$

where $f(t)$ denotes harmonic time dependence $(1, \sin t, \cos t, \cos 2t)$, T is related to the topography spectrum, S a stratification function dependent on z and A describes the influence of quasi-nonlinear advection. Note that the stratification functions S in the cross-isobath stream function obey the bottom and surface boundary condition $\hat{\psi}=0$ at $z=0, -1$. The O(1) fields in (4.6) have the following relationships:

1. Pressure functions consist of two parts. Parts containing f^2 are geostrophically related to the along-isobath flow, i.e. $ik\hat{p}=f\hat{v}$ (or $\partial p/\partial x=fv$), *in each of the harmonics* $(q=0,1,2)$.

2. The remaining part of the pressure field (independent of f) of the residual $(q=0)$ and second harmonic $(q=2)$ is a dynamic pressure correction due to advection of the first order (harmonic) flow, u, by the zeroth-order harmonic current $u^{(0)}$:

$$\hat{p}=-u^{(0)}\hat{u}.$$

Here $\hat{u}=-\partial\hat{\psi}/\partial z$ is related to the first part of the harmonic $(q=1)$ stream function field in (4.6b) only, as the second part is compensated by the barotropic part $\hat{\psi}_e=z\hat{H}\cos t$, which arises due to continuity. This has not been incorporated in (4.6b) as the emphasis is on the perturbation field. Thus $\hat{u}$ as defined here expresses the *total* horizontal, perturbation velocity.

3. The remaining part of the harmonic pressure field $(q=1)$ is related to the local accelerations of the harmonic velocity field $ik\hat{p}=-\partial\hat{u}/\partial t$, $\hat{u}$ again referring to the first part of $\hat{\psi}$ only.

Limiting situations of the expressions in (4.6) depend on the relative magnitude of three length scales contained in the stratification function S, advective function A and topography function T respectively:

(1) the baroclinic Rossby deformation radius l_i',

(2) the cross-isobath tidal excursion amplitude l_0,

(3) the topographic length scale l_τ, present in the spectral topography $\hat{H}$.

Let us briefly consider the following limits:

(i) $l_i' \ll l_0$ (weak stratification)
As before this implies $k' \to 0$ [see (4.4)]. Hence the along-isobath current $\hat{v}$ and the pressure reduce to their barotropic expressions. The stratification function, S, of the cross-isobath stream function then tends to

$$S \propto k'^2 z(z^2-1) = (l_i'/l_0)^2 k^2 z(z^2-1). \tag{4.8}$$

Thus the cross-isobath circulation is very feeble.

We can interpret $\hat{v}$, $\hat{\psi}$ and $(\partial\hat{p}/\partial x) = ik\hat{p}$ as being proportional to the spectral topography $\hat{H}$, weighted by advective functions $A_q(k)$, see Figure 1. The residual field ($q=0$) and overtide ($q=2$) have a maximum response for scales O(1), whereas the fundamental harmonic ($q=1$) has maximum response for zero k, as in barotropic studies (Zimmerman, 1980). This implies that for a *sinusoidal* topography with wave length l_τ both limits $l_0 \gg l_\tau$ and $l_0 \ll l_\tau$ give a weak response in the residual and overtide, any appreciable response being restricted to a spacing of the topography of the order of the cross-isobath tidal excursion amplitude.

(ii) $l_i' \gg l_0$ (strong stratification).
This limit corresponds to strongly stratified circumstances. The magnitude of the perturbation fields is now enhanced close to the bottom. To see this, take the limit

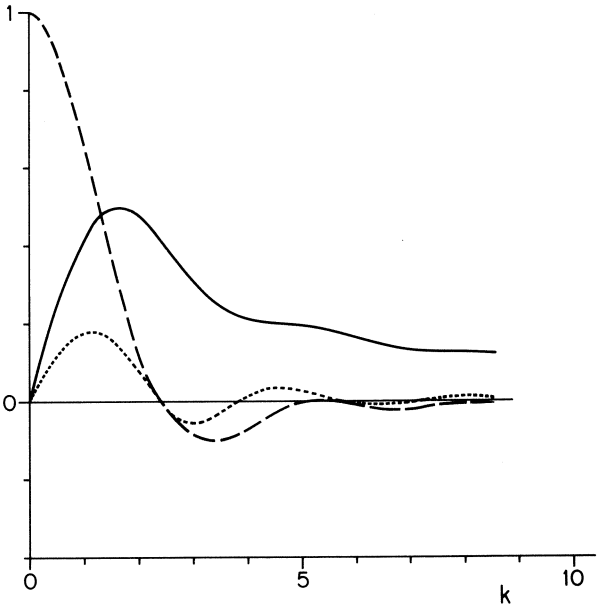

Figure 1 Advective functions $A_q(k)$: $A_0 = (-J_0^2)/k$ (——), $A_1 = 2J_0J_1/k$ (– – –), $A_2 = 2J_0J_2/k$ (----).

$k' \to \infty$. Equations (4.6) then give:

$$q=0\begin{cases}\hat{\psi}=r(-ik\hat{H})k'(z+1)e^{-k'(z+1)}\left(\dfrac{1-J_0^2}{k^2}\right),\\ \hat{v}=f(-ik\hat{H})k'\,e^{-k'(z+1)}\left(\dfrac{1-J_0^2}{k^2}\right),\\ \hat{p}=\hat{H}k'\,e^{-k'(z+1)}\left[\dfrac{1}{2}-f^2\left(\dfrac{1-J_0^2}{k^2}\right)\right],\end{cases} \tag{4.9a}$$

$$q=1\begin{cases}\hat{\psi}=-\cos t\hat{H}(e^{-k'(z+1)}+z),\\ \hat{v}=\sin tf\hat{H}k'\,e^{-k'(z+1)}2J_0J_1/k,\\ \hat{p}=\sin ti\dfrac{\hat{H}}{k}k'\,e^{-k'(z+1)}\left[1-f^2\dfrac{2J_0J_1}{k^2}\right],\end{cases} \tag{4.9b}$$

$$q=2\begin{cases}\hat{\psi}=\cos 2tr(-ik\hat{H})k'(z+1)e^{-k'(z+1)}\left(\dfrac{-2J_0J_2}{k^2}\right),\\ \hat{v}=\cos 2tf(-ik\hat{H})k'\,e^{-k'(z+1)}\left(\dfrac{-2J_0J_2}{k^2}\right),\\ \hat{p}=\cos 2t\hat{H}k'\,e^{-k'(z+1)}\left[\dfrac{1}{2}+f^2\dfrac{2J_0J_2}{k^2}\right]\end{cases} \tag{4.9c}$$

Evidently all field variables are bottom intensified in this limit. The stratification functions $S(k',z)$, implicitly defined by (4.6) and (4.7), are shown in Figure 2 for three different values of the internal Rossby deformation radius, the largest of which giving curves that approximate expressions (4.9). Apart from bottom-intensification, these curves clearly show that the cross-isobath stream function of all harmonic components increases in amplitude with increasing deformation radius. It should be noted that, although (4.6) or (4.7) show that small wavenumbers k' experience a stronger bottom intensification relative to the barotropic situation, this does not imply that for an actual topography, consisting of an infinity of wavenumbers, as discussed in the next section, it is the smallest wavenumbers that dominate the flow near the bottom. In fact it is the multiplicative effect of stratification and quasi-nonlinear advection that determines the contribution of a specific topographic wavenumber to the fields in physical space (x). This can easily be seen in (4.9). At the bottom ($z=-1$), for $\hat{v}$ and $\hat{p}$, the spectral stratification function S increases linearly as a function of k'. The total contribution of a topographic wavenumber to the field in physical space should then be considered in product with the spectral topographic amplitude T and the advection function A. Depending on the relative magnitude of $l_0/l_\tau (\ll 1$, or $\gg 1)$, k' may be rewritten as $k_\tau(l_i'/l_\tau)$, where k_τ is defined as $k_\tau \equiv k_* l_\tau$, or kl_i'/l_0. In the former case it depends on the relative magnitude l_i'/l_τ, whether or not the flow is intensified at the

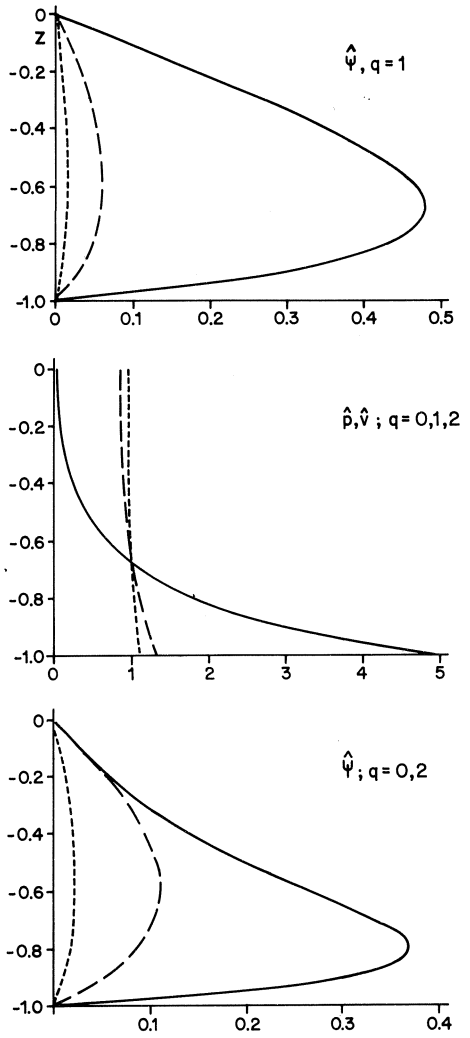

Figure 2 Stratification functions $S_{\phi,q}(z,k')$ for $k'=0.5$ (- - - - -), 1 (– – –), 5 (——); (a) $\phi=\hat{\psi}$; $q=1$, (b) $\phi=\hat{p},\hat{v}$; $q=0$, 1, 2, (c) $\phi=\hat{\psi}$; $q=0,2$.

bottom. In the latter case an unambiguous intensification is implied, with amplification factor l_i'/l_0.

The latter situation, $l_i' \gg l_0 \gg l_\tau$, is therefore the most interesting parameter range, since both quasi-nonlinear advection as well as bottom intensification are present. In the next section this will be illustrated for two specific topographies.

5. RESULTS FOR LOCALIZED TOPOGRAPHIES

In order to demonstrate the spatial structure of the topographically bounded fields we calculate the response in physical space of the dynamic field variables, discussed in the

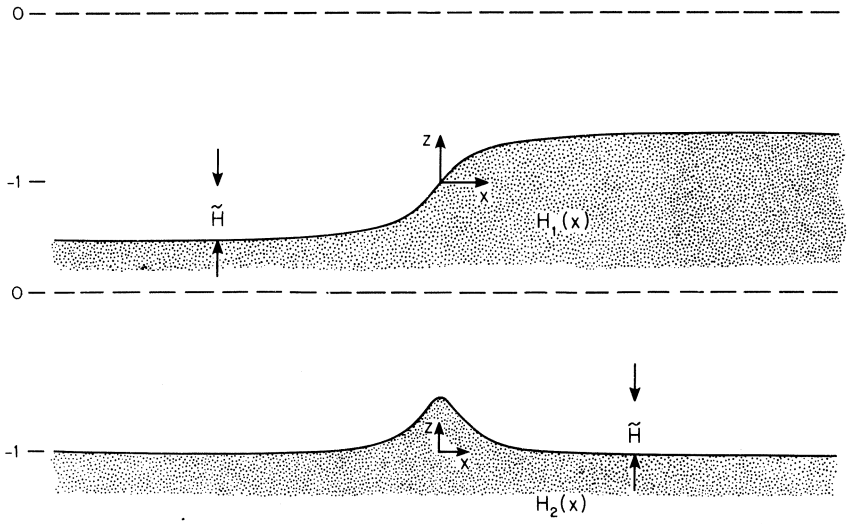

Figure 3 Topographies $H_1(x)$ and $H_2(x)$.

sections before, for two localized one-dimensional small-amplitude topographies given by:

$$H_1(x) = -\tilde{H} \arctan(x l_0/l_\tau), \tag{5.1}$$

$$H_2(x) = -\tilde{H}/[1+(x l_0/l_\tau)^2]. \tag{5.2}$$

These topographies, a step and a ridge, are shown in Figure 3. Obviously H_2 is proportional to the x-derivative of H_1. The minus signs are introduced because the perturbations, H_i, are given at $z=-(1+\delta H)$ relative to the constant reference depth $H^{(0)}=1$. Here δ is the perturbation parameter as defined in I, Equation (2.5). The non-dimensional amplitude of the topography, $\tilde{H}$, is therefore an O(1) quantity. The Fourier transformed topography spectrum reads:

$$\hat{H}_1(k) = \frac{i\tilde{H}}{2k} e^{-|k|l_\tau/l_0}, \tag{5.3}$$

$$\hat{H}_2(k) = -\frac{\tilde{H}}{2}\frac{l_\tau}{l_0} e^{-|k|l_\tau/l_0}. \tag{5.4}$$

Substitution of these expressions in (4.6) and subsequently performing the inverse Fourier transform,

$$\phi(x,z) = \int_{-\infty}^{\infty} \hat{\phi}(k,z) e^{ikx}\, dk, \tag{5.5}$$

yields the spatial structure in the cross-isobath plane (x,z) of the dynamic field variables ϕ. Since the resulting expressions (4.6) in general have no analytical inverse Fourier transform we perform this numerically in the next subsection. The most interesting limit ($l_i' \gg l_0 \gg l_\tau$) though, can be treated analytically as will be discussed in Section 5.2.

5.1 *Numerical inverse Fourier transform*

The numerical inverse Fourier transform is performed for a number of relative length scales. This is done at 8 levels in the vertical (including a bottom and surface level) and by using 1000 points in x-direction $-50 < x_*/l_0 < 50$. The results shown are for the interval $-14 < x_*/l_0 < 14$, which proved to be a convenient domain size.

The results are presented in Figure 4–12 for both topography shapes $-H_1$ (Figures 4, 6–12), H_2 (Figure 5)—various values of the topographic lengthscales l_τ (1, Figures 4–7; 0.1 Figures 8–12) and the internal Rossby deformation radius l_i' (0.1, Figure 8; 1, Figures 4–7, 9; 5, Figures 8, 10–12) relative to tidal excursion amplitude l_0 and for the three harmonic components $q=0$ (Figures 4, 5, 8, 9, 10), $q=1$ (Figures 6, 11) and $q=2$ (Figures 7, 12). In each of the figures we show from the bottom upwards:

(a) a picture of the topography used
(b) the amplitude of the along isobath velocity in the (x,z) plane (positive y direction is into the paper)
(c) the cross-isobath stream function ψ (solid curves) together with the perturbation in the pressure field in the x, z plane (dashed curves). Arrows indicate the flow direction (for time-dependent profiles at $t=0$, Figures 6, 7, 11, 12).

Dimensional magnitudes of v follow by multiplying nondimensional values, as given in the figures, by $\partial f U$. Thus a nondimensional value $v=1$ yields a dimensional along-isobath velocity $v_* = 8\ \mathrm{cm\ s^{-1}}$, for a velocity amplitude $U = 1\ \mathrm{m\ s^{-1}}$, a ratio of internal and external length scale $\delta = 0.1$ and a typical midlatitude value of the Coriolis parameter $f = f_*/\sigma(M_2) = 0.8$, say. Dimensional stream function values follow by multiplying ψ with $\delta H_0 U$. Its derivatives $\partial\psi_*/\partial x_*$ and $-\partial\psi_*/\partial z_*$ give the corresponding dimensional velocities. The interpretation of nondimensional pressure field values is ambiguous. Formally a dimensional value is obtained by multiplying it with $\delta^3 H_0 \bar{\rho}_* g$, i.e. δ^3 times the hydrostatic head at the sea floor. More often, however, its values are interpreted in terms of an equivalent sea surface elevation $\zeta_* = p_*/(\bar{\rho}_* g)$. Since the scale of ζ: $Z = \delta H_0$, this still renders small values of order $\zeta = \zeta_*/Z = \delta^2 p$. Alternatively pressure variations may be due to internal isopycnal deviations $\zeta_{i*} = p_*/(\rho'_* g)$. Since $\rho'_* = \delta^2 \bar{\rho}_*$ (I; 2.5) internal deformations $\zeta_i = \zeta_{i*}/Z = p$. Therefore nondimensional O(1) pressure values may also be interpreted as giving interface deformations of order of magnitude Z.

We start by considering the most balanced situation in which all length scales have similar magnitudes:

(i) $l_i' = l_0 = l_\tau$.

Figure 4 gives the perturbation fields for topography $H_1(x)$ for the residual ($q=0$) motion. The residual along-isobath jet (Figure 4b) obtains a maximum value of 0.48 at the bottom. Especially at the slope the inhibitive effects of stratification are evident, say for $|x_*/l_0| \leqslant 0.6$. Outside this region the residual jet is almost vertically uniform. The residual cross-isobath circulation (Figure 4c) consists of a three cell pattern with *down slope* velocities near the bottom of the middle cell. The pressure structure (Figure 4c) is dominated by the barotropic "Bernoulli head".

The residual patterns for the topography $H_2(x)$ (Figure 5) are a logical extrapolation of those obtained for a single slope. The residual jets point in opposite direction on

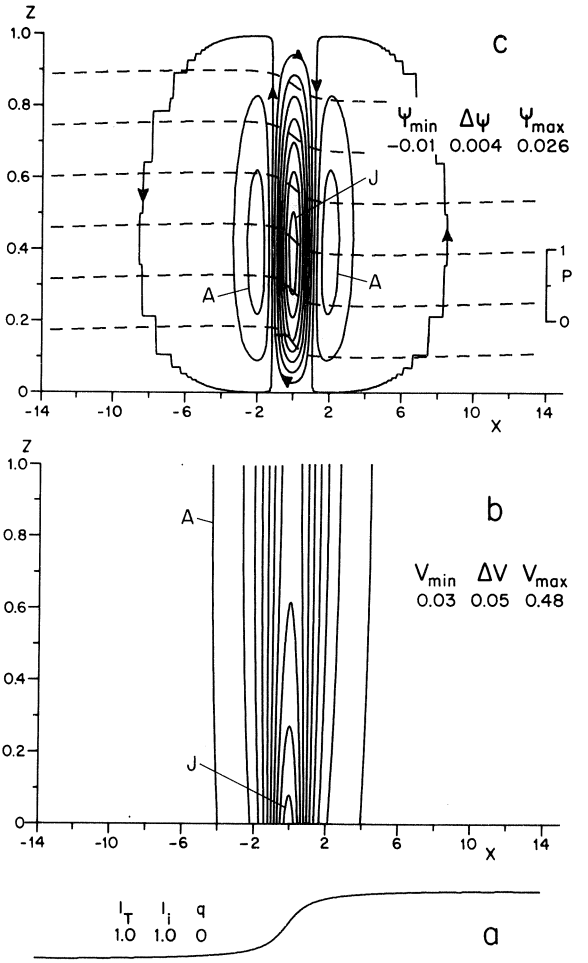

Figure 4 Topography (a), along-isobath velocity (b) and streamfunction (solid lines) and pressure field (dashed lines) (c) as a function of $x=x_*/l_0$ and $z=z_*/H_0$ for the residual component, $q=0$, and $l_T=l_t/l_0=1.0$, $l_i=l_i'/l_0=1.0$. Ten contours are shown ranging from $V_{\min}$ and $\Psi_{\min}$ (label A) to $V_{\max}$ and $\Psi_{\max}$ (label J) in steps ΔV and $\Delta\Psi$. The pressure scale is indicated at the right hand side of the top figure (in nondimensional values) and its interpretation is discussed in the text. The stream function field shown is divided by the small damping parameter r.

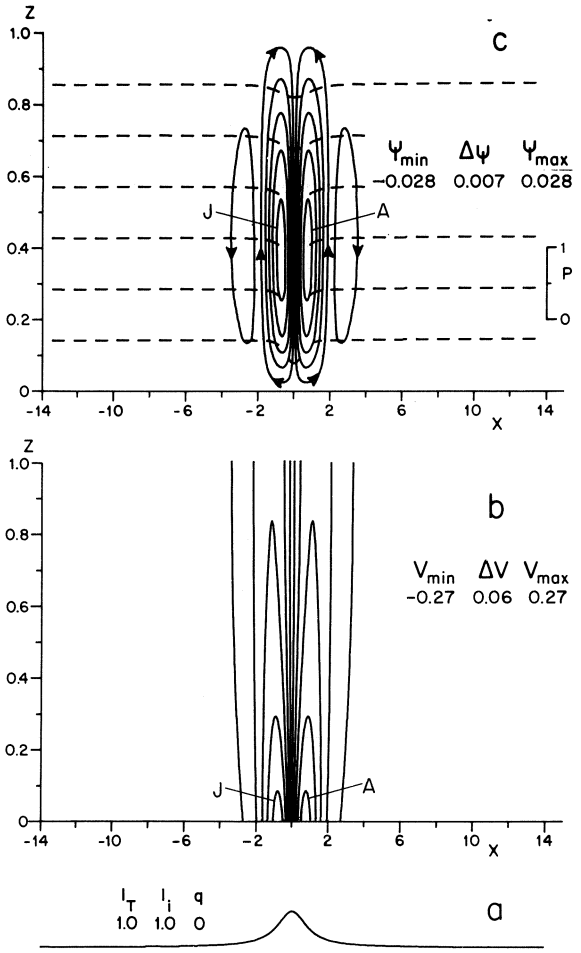

Figure 5 As figure 4, for $H_2(x)$.

both sides of the bank, such that the circulation around isolated banks is anti-cyclonic. The cross-isobath stream function now consists of four cells, with strong downwelling above the bank, since the two weaker side cells of the single slope topography have merged together. The fact that topography H_2 is simply the derivative of H_1 is reflected in the symmetry of the figures with respect to $x=0$. That is, whenever one of the topographies gives a symmetric distribution of a field variable, the other topography gives an anti-symmetric distribution. This means that if the shape of a field variable for one of the two topographies is given, the shape for the other can simply be inferred. Thus from hereon we shall only discuss the results for a step topography in more detail. It should be noted, however, that the (anti)symmetry of the results for a step topography rests on working in the small topographic amplitude limit. Finite amplitude effects generally shift the strongest effects to the shallower side of the step as in the barotropic case (Loder, 1980).

Results for the fundamental frequency $q=1$ are shown in Figure 6. The horizontal variations in along-isobath velocity should be interpreted as being largely due to the local depth change. Here also inhibitive stratification effects are concentrated near the origin. The stream function field (Figure 6c) oscillates in phase with the basic tidal current. No pressure field is shown for fields oscillating harmonically in time ($q=1$), Figures 6 and 11, as it contains a component increasing linearly with x. This is associated with a uniform pressure gradient (oscillating in time), which is mirroring perturbations in tidal velocity amplitude on and off the "shelf" due to (perturbational) changes in depth.

The second harmonic, M_4 say, shown in Figure 7, gives a picture that is quite similar to that of the residual component as shown in Figure 4, although a little more spreaded around the step and therefore a little weaker in magnitude.

(ii) $l_\tau/l_0 \ll 1, \quad 0 < l_i'/l_0 < \infty$

Although advective factors in the spectral response functions (4.6a,c) give the strongest response for topographic wavelengths of the order of the tidal excursion, the response in physical space has a maximum when the topography approaches a real step, i.e. when $l_\tau/l_0 \to 0$ (relative to the tidal excursion amplitude) as has been discussed by Zimmerman (1981). From hereon we therefore discuss some further results in the

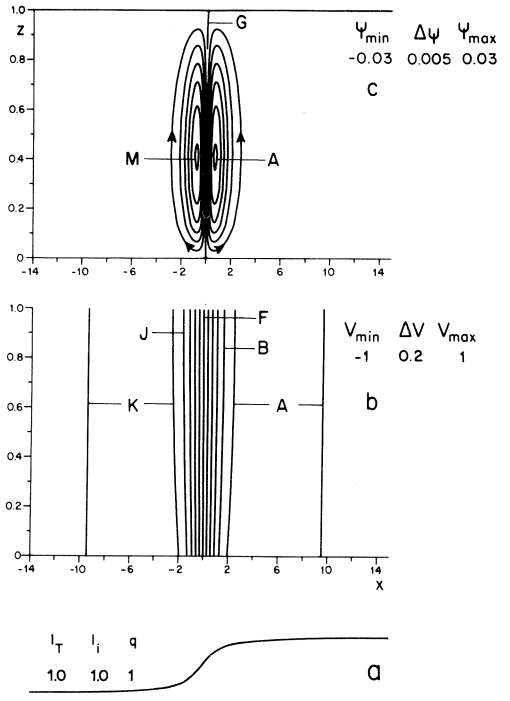

Figure 6 As Figure 4, $q=1$; eleven (Figure 6b) and thirteen (Figure 6c) contours are shown, labeled through to K and M respectively.. The stream function field is not divided by r, as for $q=0$.

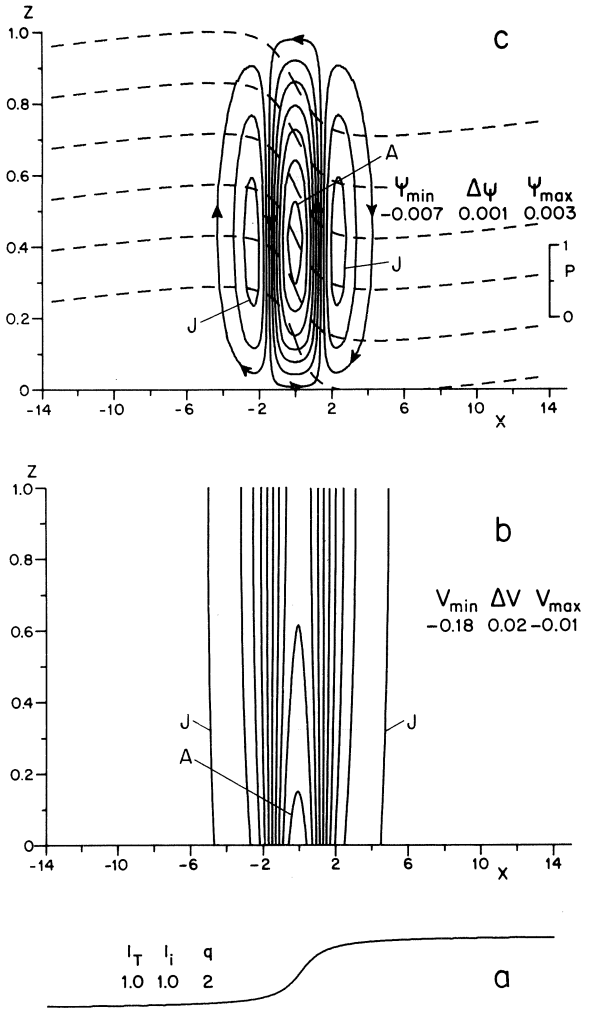

Figure 7 As Figure 4, $q=2$.

strongly responsive limit $l_\tau/l_0=0.1$. Then the only free parameter left is the internal Rossby deformation radius l_i', measuring the influence of stratification. Figures 8–10 show the residual component for a sequence of increasing l_i'. The results corroborate our earlier conclusions for the spectral amplitudes of the dynamic field variables: strong bottom-intensification for large values of the deformation radius, both in the along isobath velocity and in the cross-isobath stream function and a weakening of the latter when the barotropic limit is approached. In this limit (Figure 8) the along-isobath jet is vertically uniform, being limited exactly to the range $|x_*/l_0| \leqslant 2$, whereas it has a dimensionless maximum value of $4/\pi$. This is all in accordance with the results of Maas *et al.* (1987) for a step profile. The pressure field, although almost barotropic,

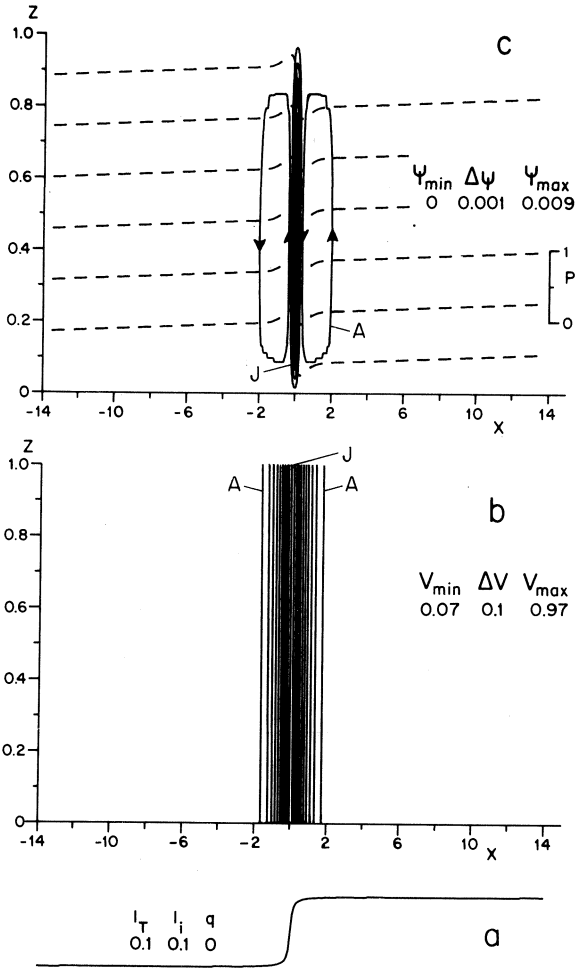

Figure 8 As Figure 4, $l_i=0.1$, $l_T=0.1$.

now clearly demonstrates the two parts of which it consists (Maas, 1987):

1. the "global" Bernoulli part mirroring the bottom profile;
2. the "local" geostrophically adjusted trapped part with its characteristic "discontinuity" at the origin (Gill, 1982).

Also the latter part becomes bottom intensified for strong stratification as Figure 10 clearly shows.

In Figures 11 and 12 we present the results for the first, $q=1$, and second, $q=2$, harmonic components in the case of strong stratification ($l_i'/l_0=5$). These also show the now familiar property of bottom trapping, most curiously in Figure 12 where the along-isobath velocity component of the overtide (M_4) has a four-cell structure near

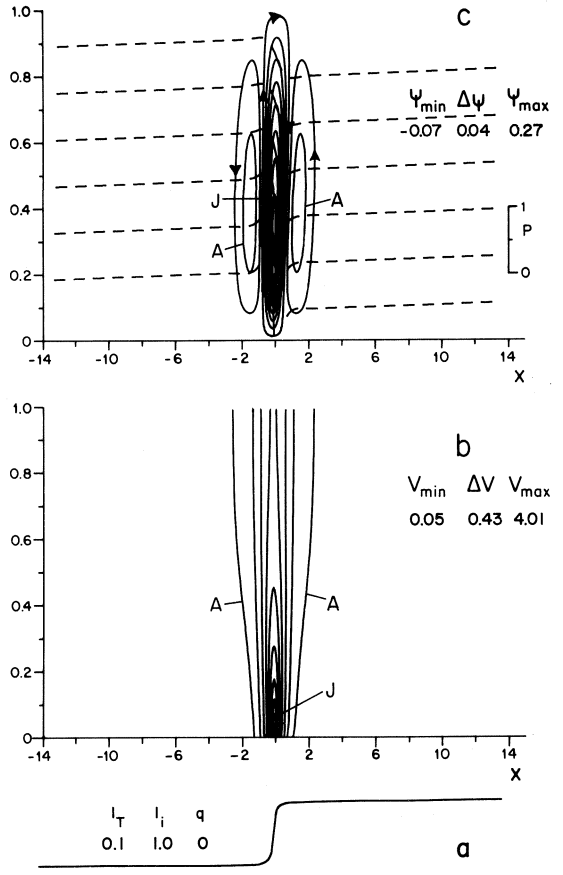

Figure 9 As Figure 4, $l_T = 0.1$

the bottom and a three-cell structure higher up in the watercolumn. This points to an effect already mentioned before: different topographic wavenumbers add-up with different weight depending on the vertical coordinate in the final inverse Fourier transformation.

In fact the limit considered here, $l_\tau/l_0 \to 0$ and $l_0/l_i' \to 0$, can be evaluated analytically as is demonstrated in the next subsection.

5.2. *Analytical inverse Fourier transform*

As pointed out, each expression in (3.10) contains, besides a time-dependent function, a topographic ($\propto \hat{H}$), a stratification ($\propto k'$), and an advective ($\propto$ Bessel functions) function. Most of these spectral functions decay to zero as k approaches infinity. The spectral function decreasing fastest, however, will determine the response. For a step-topography, (5.1) with $l_\tau/l_0 \to 0$ as we will consider here, the spectral slope is given by

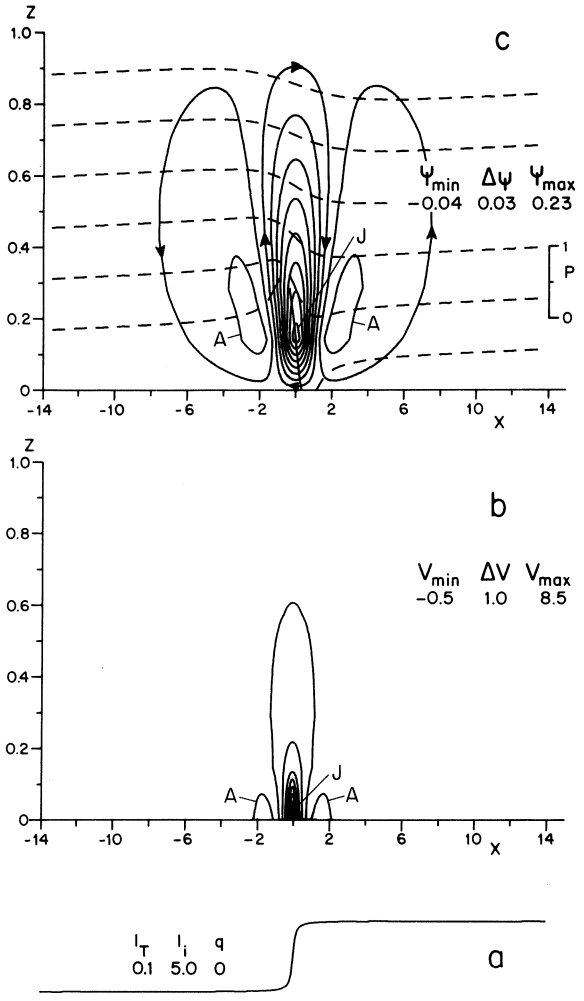

Figure 10 As Figure 4, $l_T=0.1$, $l_i=5$.

[see (5.3)]:

$$ik\hat{H}=\lim_{l_\tau/l_0\to 0}-\frac{\hat{H}}{2}\exp[-|k|l_\tau/l_0]=-\frac{\tilde{H}}{2}, \tag{5.6}$$

a constant. Similarly the argument, k, of advective functions $A_q(k)$ can be rewritten in terms of k' as $k=k'l_0/l_i'$, which, as we consider $l_0/l_i'\to 0$, approaches zero. Thus from the asymptotic behaviour (A3) of the Bessel functions, the advective functions also become constant and stratification functions dominate the response.

For convenience denote the harmonic dependence (q) as a subscript, e.g. p_{0n} referring to the nth vertical mode of the residual ($q=0$) pressure field p_0. Then, from

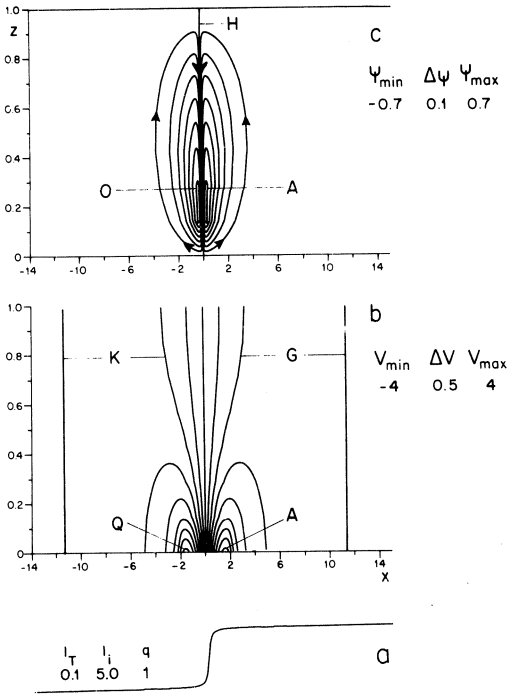

Figure 11 As Figure 4, $q=1$, $l_T=0.1$, $l_i=5$; seventeen (Figure 11b) and fifteen (Figure 11c) contours are shown, labeled through to Q and O respectively. The stream function field is divided by r, as for $q=0$.

(3.10) and (5.6), the spatial dependence of p_0, p_2 and v_1 is given by the same function s [defined in (5.7)] $p_0, p_2, v_1 \propto$

$$-\frac{\tilde{H}}{2}\left[\int_{-\infty}^{\infty}\frac{\sin k'x'}{k'}\,dk' + 2\sum_{n=1}^{\infty}\cos n\pi(z+1)\int_{-\infty}^{\infty}\frac{k'}{n^2\pi^2+k'^2}\sin k'x'\,dk'\right],$$

where we used an x-coordinate scaled with the internal Rossby deformation radius: $x'=x_*/l_i'=xl_0/l_i'$. The integrals can be evaluated as (Gradshteyn and Ryzhik, 1980, p. 1150):

$$p_0, p_2, v_1 \propto -\pi\tilde{H}\,\mathrm{sgn}(x')\left[1+2\sum_{n=1}^{\infty}e^{-n\pi|x'|}\cos n\pi(z+1)\right],$$

which series is summed (Oberhettinger, 1973) as

$$\frac{1}{\tilde{H}}(p_0, p_2, v_1) \propto s(\tilde{x},\tilde{z}) \equiv -\pi\frac{\sinh\tilde{x}}{\cosh\tilde{x}-\cos\tilde{z}}, \tag{5.7}$$

in terms of

$$\tilde{x}\equiv\pi x'=\pi x_*/l_i', \qquad \tilde{z}\equiv\pi(z+1). \tag{5.8}$$

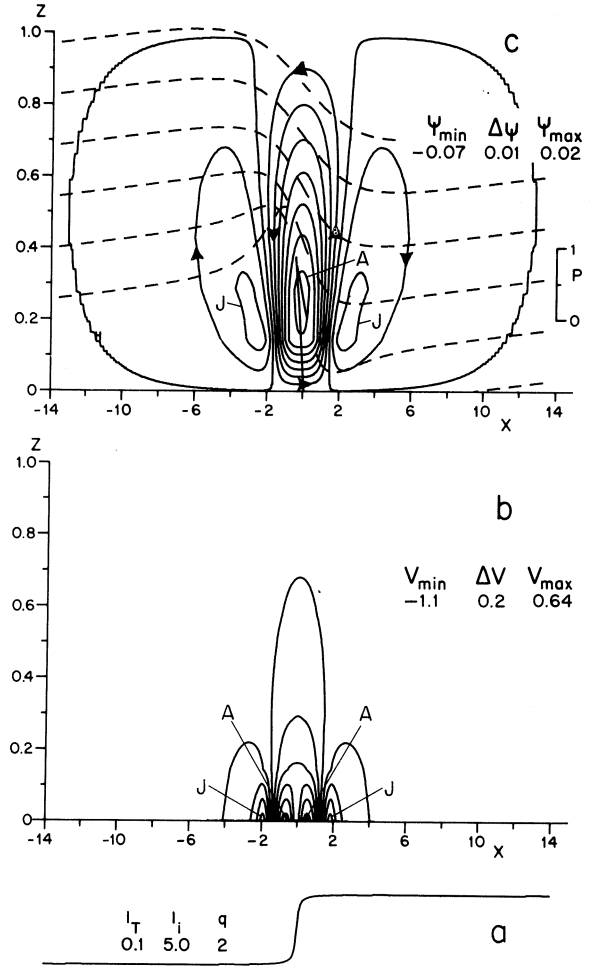

Figure 12 As Figure 4, $q=2$, $l_T=0.1$, $l_i=5$.

One may check that this spatial field conforms with those sketched in Figure 10c, 11b, 12c for p_0, v_1 and p_2 respectively. The function $s(\tilde{x},\tilde{z})$ defined in (5.7), has the following characteristics:

1. at the surface $\tilde{z}=\pi$ $(z=0)$, $s(\tilde{x},\pi)\to -\pi\tanh\tilde{x}/2$,
2. at middepth $\tilde{z}=\pi/2$ $(z=-1/2)$, $s(\tilde{x},\pi/2)\to -\pi\tanh\tilde{x}$,
3. at the bottom $\tilde{z}=0$ $(z=-1)$, $s(\tilde{x},0)\to -\pi/\tanh\tilde{x}/2$,
4. near the origin $\tilde{x},\tilde{z}\to 0$ $(x\to 0, z\to -1)$,

$$\lim_{\tilde{x},\tilde{z}\to 0} s=\lim_{\tilde{x}\to 0} 2\pi\frac{-\tilde{x}}{\tilde{x}^2+\tilde{z}^2}=-2\pi^2\delta(\tilde{z}),$$

which indicates a singularity in the residual and second harmonic pressure fields (p_0 and p_2). From (5.5), applied at $x=0$, we conclude that the value of a field at the origin is finite when its spectrum drops to zero at infinity. The apparent singularity in v_1 is therefore checked by its spectral advective part. The behaviour in Case 2 above is also governing the spatial structure in the far field ($|\tilde{x}| \to \infty$), the finite values of which express the way the perturbation analysis is mirroring the perturbation in depth.

The spatial structure of the harmonic pressure field p_1 is an integral of $s(\tilde{x}, \tilde{z})$ given in (5.7). Thus

$$p_1 \propto \pi \tilde{H}(l_i'/l_0) \ln [\cosh \tilde{x} - \cos \tilde{z}]. \tag{5.9}$$

In the near field p_1 is a logarithmic function of the radial coordinate $\rho = (\tilde{x}^2 + \tilde{z}^2)^{1/2}$

$$\lim_{\tilde{x},\tilde{z} \to 0} p_1 \propto \ln \rho.$$

which again expresses a perturbative correction to the zeroth order, driving pressure field.

The spatial structure of the residual and second harmonic along-isobath velocities are determined by the horizontal derivative of s

$$v_0, v_2 \propto \frac{l_o}{l_i'} \frac{1 - \cosh \tilde{x} \cos \tilde{z}}{(\cosh \tilde{x} - \cos \tilde{z})^2}. \tag{5.10}$$

In the near field v_0 and v_2 approach

$$\frac{l_0}{l_i'} \frac{\tilde{z}^2 - \tilde{x}^2}{(\tilde{z}^2 + \tilde{x}^2)^2}, \tag{5.11}$$

which indicates a flow reversal for $|\tilde{x}| > \tilde{z}$ (Figure 10b). Since v_0 and v_2 have a small coefficient, l_0/l_i', in front of their spatial structure function this suggests that the flows are weak, in contradiction with earlier remarks about intensification. This paradox is resolved by considering that (5.10), or (5.11), have a singularity near the origin, their true values being determined by their spectral advective parts (neglected in this subsection). This is also suggested by the structure of v_2 at the bottom in Figure 12b. Bottom intensification, as discussed in Section 4, therefore still holds.

The spatial stream function fields ψ_0 and ψ_2 can be obtained in the same way:

$$\psi_0, \psi_2 \propto \frac{l_0}{2l_i'} \frac{\sin \tilde{z}}{(\cosh \tilde{x} - \cos \tilde{z})^2} [\cosh \tilde{x} - \cos \tilde{x} - \tilde{x} \sinh \tilde{x}]. \tag{5.12}$$

In the near field this reduces to

$$\psi_0, \psi_2 \propto \frac{l_0}{l_i'} \sin \tilde{z} \frac{\tilde{z}^2 - \tilde{x}^2}{(\tilde{z}^2 + \tilde{x}^2)^2},$$

which expresses the three cell structure observed in Figure 10c and 12c and which satisfies the boundary conditions at $\tilde{z}=0,\pi$.

The harmonic spatial stream function field finally is proportional to

$$\psi_1 \propto -\mathrm{sgn}(\tilde{x})\frac{2}{\pi}\arctan\left(\frac{\sin\tilde{z}}{\exp|\tilde{x}|-\cos\tilde{z}}\right), \tag{5.13}$$

which may be compared with the pattern in Figure 11c. It consists of a very localized downwelling at the centre and broad upwelling regions at its sides. This downwelling is annihilated by directly forced vertical flow, associated with $\hat{\psi}_{e,1}=z\hat{H}\cos t$, not included here, as we verify below.

The spectral harmonic total vertical velocity, valid for any value of the cross-isobath tidal excursion, is, from (4.6b), given by

$$\hat{w}_{\text{total}}=ik\hat{\psi}_{\text{total}}=ik(\hat{\psi}_1+\hat{\psi}_{e,1})=ik\hat{H}\cos t\frac{\sinh k'z}{\sinh k'}, \tag{5.14}$$

which, in the limit $l_i'/l_\tau\to 0$, reduces to the barotropically forced vertical velocity

$$w_{\text{total}}\to z(dH/dx)\cos t=w_e.$$

For the step-topography then, vertical velocities are very localized:

$$w_{\text{total}}\to -\pi z\tilde{H}\,\delta(x)\cos t. \tag{5.15}$$

The inverse Fourier transform of (5.14) reads (Gradshteyn and Ryzhik, 1980, p. 1152)

$$w_{\text{total}}=\pi\frac{\tilde{H}}{2}\cos t\frac{l_0}{l_i'}\frac{\sin\tilde{z}}{\cosh\tilde{x}-\cos\tilde{z}}, \tag{5.16}$$

which is everywhere positive (at the initial time $t=0$). This demonstrates that the downwelling at $x=0$, of the induced vertical velocity is offset by its directly forced counterpart. As $\tilde{x}$, $\tilde{z}\to 0$,

$$w_{\text{total}}\to\pi\tilde{H}\cos t\frac{l_0}{l_i'}\frac{\tilde{z}}{\tilde{x}^2+\tilde{z}^2}=\pi\tilde{H}\cos t\left(\frac{1}{\pi}\frac{z'}{x^2+z'^2}\right),$$

where $z'\equiv\tilde{z}l_i'/(l_0\pi)$. Since the bracketed part in this equation is just one of the definitions of the Dirac delta function, $\delta(x)$, as $z'\to 0$, this shows that the vertical velocity is reducing to the externally imposed velocity at the origin $(x,z'=0)$, $w_e(z=-1)$, see (5.15). In general, however, the vertical velocity field (5.16) is much less localized as compared to its barotropic counterpart, (5.15). This is due to the internal geostrophic adjustment, which takes place in response to the localized forcing.

6. DISCUSSION AND CONCLUSIONS

Although the results for a stratified fluid have much in common with those for topographically bounded motion in a homogeneous, barotropic flow, there are several remarkable differences that are due to baroclinicity. First there is the phenomenon of bottom intensification, depending on the internal Rossby deformation radius, l_i'. This is reminiscent of topographic Rossby waves in a stratified fluid (Rhines, 1970) which also show bottom trapping depending on l_i'. Indeed the forced motions discussed here and the free modes discussed by Rhines (1970) can both be thought of as manifestations of potential vorticity conservation. Actually the vertical components of relative vorticity, ω_z, in the present context obeys (for bottom friction dominating internal friction):

$$\frac{d}{dt}\omega_z + E_-^{1/2}\omega_z = f\left(-u_0\frac{dH}{dx} - \frac{\partial w_i}{\partial z}\right), \tag{6.1}$$

where

$$\omega_z = \frac{\partial v}{\partial x}. \tag{6.2}$$

As in the barotropic problem (Zimmerman, 1978, 1980; Huthnance, 1981; Robinson, 1983) relative vertical vorticity is produced by stretching of planetary vortex lines. However, apart from the depth-independent externally imposed stretching by the interaction of topography and the barotropic tide (first term in the right-hand side of (6.1)) there now is the depth-dependent stretching due to the free internal modes (second term in the right-hand side of (6.1)). It is the latter effect that produces bottom trapping, as for the topographically bounded internal modes, discussed here, the vertical structure of the internal motions is exponential rather than sinusoidal.

A second feature, absent in two-dimensional (vertically averaged) barotropic theory is the occurrence of cross-isobath circulation, being bottom intensified as well. Moreover the cross-isobath circulation in contrast to the along-isobath velocity does not vanish for $f \to 0$. As for frictionally induced vertical structure of barotropic topographically bounded currents (Zimmerman, 1986), the baroclinic vertical structure can be discussed in terms of the horizontal vorticity components, $\omega_{x,y}$. For a fluid in hydrostatic balance we have:

$$(\omega_x, \omega_y) = \left(\frac{\partial v}{\partial z}, -\frac{\partial u}{\partial z}\right). \tag{6.3}$$

In the present context these components obey:

$$\frac{d}{dt}\omega_x - f\omega_y + E_-^{1/2}\omega_x = 0 \tag{6.4}$$

$$\frac{d}{dt}\omega_y + f\omega_x + E_-^{1/2}\omega_y = \frac{\partial \rho}{\partial x} \tag{6.5}$$

whereas

$$\frac{d}{dt}\rho - w_i N^2 = z u_0(t)\frac{dH}{dx} N^2 \equiv F(x, z, t). \tag{6.6}$$

Hence (6.5) can be transformed into

$$\frac{d^2}{dt^2}\omega_y + f\frac{d\omega_x}{dt} + E^{1/2}\frac{d\omega_y}{dt} = \frac{\partial}{\partial x}[F - w_i N^2]. \tag{6.7}$$

The forcing term in the right-hand side of (6.7) describes the solenoidal generation of horizontal vorticity, a genuine baroclinic effect. Evidently the x-component of horizontal vorticity, which describes the occurrence of vertical shear in the along-isobath currents, is derived from the y-component of the horizontal vorticity, describing circulation in the cross-isobath plane, by coupling via the Coriolis parameter; i.e. tilting of planetary vorticity by shear in the cross-isobath flow [see (6.4)]. That mechanism is absent for $f = 0$, as is the stretching of planetary vorticity described in (6.1). Hence for $f = 0$ no along-isobath currents occur. However, as (6.7) shows, in the absence of tilting of planetary vorticity by shear in the along-isobath current [second term in the left-hand side of (6.7)], there still is the solenoidal generation of y-vorticity in the right-hand side of (6.7) which does not vanish for $f \to 0$. Quasi-nonlinear advection may transfer that vorticity in frequency space both to the residual and the higher harmonics.

It should be interesting to compare the sense of the cross-isobath Eulerian circulation due to baroclinicity with that due to bottom friction. Unfortunately results for the latter (Wright and Loder, 1985; Tee, 1985; Yasuda and Zimmerman, 1986) are very sensitive to the parametrization of bottom friction and to the formulation of the bottom boundary conditions. For a ridge topography (Figure 5), the induced downslope residual circulation at the bottom accords with the results of Yasuda and Zimmerman (1986) for a similar topography when $f/\sigma \to 1$. Thus for a ridge both mechanisms can be reinforcing. For a step—Figures 4, 8, 9, 10—our results show a downslope residual bottom current at the position of the steepest slope and an upslope bottom current on the shallower side. However, for an asymmetric topography as a step, finite-amplitude effects, which shift the cross-isobath circulation to the shallow side of the step (Tee, 1985), obscure a comparison. Wright and Loder (1985) conclude for a large variety of parameter ranges that residual cross-isobath circulation has a bias towards bottom currents going up-slope. It is however hard to construct a cross-isobath circulation pattern for a real step topography from their results, since these are derived as local approximations. However, the results of Tee (1985) for finite amplitude step-topographies at Georges Bank may be compared with ours, particularly for the northern section where the along-isobath residual current has a jet-like structure, as in our small-amplitude step topography. It is interesting to observe that Tee's model, as ours, gives a three-cell structure for the cross-isobath residual circulation. Going from deep to shallower water, the three cells have the same circulation sense as in Figures 4, 8, 9, 10, i.e. anticlockwise, clockwise, anticlockwise. An interesting difference is the

position of these cells with respect to the maximum of the along-isobath current. In our pictures, the middle cell is located exactly at the along-isobath jet's axis. In Tee's (1985) picture that axis coincides more or less with the boundary between the middle and the shallower cell. A recent calculation of higher order advective effects (Tang and Tee, 1987) shows that this probably is not a result of an improper representation of advective effects in a weakly nonlinear model, as these effects only shift the whole structure to deeper waters. Thus either the difference in location of the cross-isobath circulation cells is due to a difference in dynamics between bottom-frictionally induced and baroclinically induced vertical structure, or the difference is due to dealing with a finite or a small amplitude topography. A downslope cross-isobath Eulerian current is also observed in a model where the mean flow is driven by a tidally induced buoyancy flux (Ou and Maas, 1986). In their model stratification acts in a similar way as friction in the wave-mean flow theories, referred to above, in the sense that its incorporation ($N^2 \neq 0$) provides the necessary phase-shift among oscillating components to produce a non-zero momentum transfer from the oscillatory to the mean motion. The actual mean flow however is independent of its precise magnitude. Moreover it again depends crucially on the frictionally induced vertical phase differences of the driving tidal field, as in the above theories. This is distinguishing it from the model considered presently, where the zeroth order tidal field is depth-independent, which implies that the resulting fields may at times be additive.

Both Wright and Loder (1985) and Tee (1985) observe a strong influence of the Stokes drift on the Lagrangian cross-isobath residual circulation. The latter can be much weaker than the former, whereas sometimes the sense of the circulation is reversed compared to the Eulerian pattern. This is in accordance with our small-amplitude result, which predicts an exact vanishing of the Lagrangian residual circulation, the Eulerian being completely offset by the Stokes drift.

Finally, the results in Figures 9–12 for a sharp step, show that the along-isobath velocity field (and the other dynamic variables as well) are not confined exactly to a strip of two times the tidal excursion on both sides of the step, as is the case in the barotropic situation shown in Figure 8 (Maas *et al.*, 1987). This is not an artefact of the numerical procedure for the inverse Fourier transformation or of an approximate representation of the step-function ($l_\tau/l_0 = 0.1$ and not $l_\tau \to 0$), which can be seen as follows. The occurrence of the along-isobath velocities is due to planetary vortex stretching by the total vertical motion induced by the topography, as the right-hand side of (6.7) shows. As (5.14) reveals, the total vertical velocity is exactly confined to the step in the limit of vanishing stratification. Hence, any vertical vorticity that is produced by planetary vortex stretching can at most be spread out by advection over a distance of two times the tidal excursion amplitude, analogously to the situation in the barotropic case (Maas *et al.*, 1987), to which it effectively reduces. In the other extreme ($l_i'/l_0 \gg 1$), however, the total vertical velocity ($w_{\text{total}} = w_i + w_e$), Eq. (5.16), has an exponential distribution, around the step,

$$\lim_{|\tilde{x}| \gg 1} w_{\text{total}} = \pi \tilde{H} \cos t \frac{l_0}{l_i'} \exp(-|\tilde{x}|) \sin \tilde{z}.$$

This describes the geostrophically trapped part of the internal adjustment that takes

place in response to the forcing. Its effect is not confined exactly to an interval around the step. In fact, as $\tilde{x}$ is the dimensional X_* scaled with the internal Rossby deformation radius, it is the internal Rossby deformation radius that determines the *e*-folding distance. Thus baroclinic along-isobath currents exhibit exponential decay around a step and therefore they may be found at greater distances than their barotropic counterpart.

The final question now is whether there is any observational support for the existence of topographically bounded, bottom intensified internal tides and residual currents. Obviously two features should at least be present in observations: bottom intensification and residual currents and/or higher harmonics, M_4 say. To our knowledge only the data from the continental slope near northwest Africa as discussed by Gordon (1980) and Huthnance and Baines (1982) meet those criteria. Although no residuals are reported, the internal tide is bottom intensified and particularly in the cross-isobath direction, shows the occurrence of overtides, especially M_4. Unfortunately, we certainly are dealing with a finite amplitude topography there. Bottom intensification of internal tides then may also be explained in terms of the wave characteristics for internal tides. Whenever the slope of the topography equals that of the wave characteristic, bottom intensification will occur. Gordon (1980) suggests that this is indeed the case, both for the M_2 and the M_4 components, whereas Huthnance and Baines (1982) support that suggestion only for M_4 and remain inconclusive about the explanation of bottom intensification of the M_2 tidal currents. Whether or not the topographically bounded modes discussed here can explain some of these features is hard to assess due to the difference in dynamics for small-amplitude and finite-amplitude topographies. We are evidently in need of a (quasi)nonlinear theory for internal tides over finite-amplitude topographies. For the time being, therefore, the mechanism we have presented here for bottom intensification of internal tides is just a concurrent one to other possibilities.

REFERENCES

Gill, A. E., *Atmosphere-Ocean Dynamics*, Academic Press, New York (1982).

Gordon, R. L., "Tidal interactions in a region of large bottom slope near north-west Africa during JOINT-1". *Deep-Sea Res.* **25**, 625–643 (1980).

Gradshteyn, I. S. and Ryzhik, I. M., *Table of integrals, series and products*, Academic Press, New York (1980).

Huthnance, J. M., "Tidal current assymetries over the Norfolk sandbanks", *Estuar. Coast. Mar. Sci.* **1**, 89–99 (1973).

Huthnance, J. M., "On mass transport generated by tides and long waves", *J. Fluid Mech.* **102**, 367–387 (1981).

Huthnance, J. M. and Baines, P. G., "Tidal currents in the northwest African upwelling region", *Deep-Sea Res.* **29**, 285–306 (1982).

Loder, J.W., "Topographic rectification on the sides of Georges Bank", *J. Phys. Oceanogr.* **10**, 1540–1551 (1980).

Loder, J. W. and Wright, D. G., "Tidal rectification and frontal circulation on the sides of Georges Bank", *J. Mar. Res.* **43**, 581–604 (1985).

Maas, L. R. M., "Tide-topography interactions in a stratified shelf sea", Ph.D. Thesis, Univ. Utrecht (1987).

Maas, L. R. M., Zimmerman, J. T. F. and Temme, N. M., "On the exact shape of a topographically rectified tidal flow", *Geophys. Astrophys. Fluid Dyn.* **38**, 105–129 (1987).

Maas, L. R. M. and Zimmerman, J. T. F., "Tide-topography interactions in a stratified shelf sea", I: Basic equations for quasi-nonlinear internal tides", *Geophys. Astrophys. Fluid Dyn.* **45,** 1–35 (1989).

Maas, L. R. M. and Zimmerman, J. T. F., "Tide-topography interactions in a stratified shelf sea, III: quasi-nonlinear gravity wave modes", in preparation for submission to Geophys. Astrophys. Fluid Dyn. (1989).

Oberhettinger, F., *Fourier expansions*, Academic Press, New York (1973).

Ou, H. W. and Maas, L. R. M., "Tidal-induced buoyancy flux and mean transverse circulation", *Cont. Shelf Res.* **5,** 611–628 (1986).

Rhines, P. B., "Edge- bottom- and Rossby waves in a rotating stratified fluid", *Geophys. Fluid Dyn.* **1,** 273–302 (1970).

Robinson, I. S., "Tidally induced residual flow", in: B. Johns (ed.) *Physical Oceanography of coastal and shelf seas*, Elsevier, Amsterdam, 321–357 (1983).

Tang, Y. and Tee, K. T., "Effects of mean and tidal current interaction on the tidally induced residual current", *J. Phys. Oceanogr.* **17,** 215–230 (1987).

Tee, K. T., "Depth-dependent studies of tidally induced residual currents on the sides of Georges Bank", *J. Phys. Oceanogr.* **15,** 1818–1846 (1985).

Wright, D. G. and Loder, J. W., "A depth-dependent study of the topographic rectification of tidal currents", *Geophys. Astrophys. Fluid Dyn.* **31,** 169–220 (1985).

Yasuda, H. and Zimmerman, J. T. F., "Tide-induced residual currents with Stokes and Ekman layers over an undulatory sea floor", *J. Oceanogr. Soc. Japan* **42,** 276–293 (1986).

Zimmerman, J. T. F., "Topographic generation of residual circulation by oscillatory (tidal) currents", *Geophys. Astrophys. Fluid Dyn.* **11,** 35–47 (1978).

Zimmerman, J. T. F., "Vorticity transfer by tidal currents over an irregular topography", *J. Mar. Res.* **38,** 601–630 (1980).

Zimmerman, J. T. F., "Topographical rectification: a comment on spectral representation", *J. Phys. Oceanogr.* **11,** 1037–1039 (1981).

Zimmerman, J. T. F., "Principal differences between 2d and vertically averaged 3d models of topographically rectified tidal flow", *Lect. notes Coastal Estuar. Stud.* (ed. J. van de Kreeke) **16,** 120–129 (1986).

APPENDIX

Relations for Bessel functions of the first kind, $J_n(k)$

1. Addition and subtraction rules

$$\left.\begin{aligned} J_{m-1}(k)+J_{m+1}(k)&=2\frac{m}{k}J_m(k),\\ J_{m-1}(k)-J_{m+1}(k)&=2\frac{d}{dk}J_m(k). \end{aligned}\right\} \tag{A1}$$

2. Infinite series involving Bessel functions

$$\left.\begin{aligned} &\lim_{\varepsilon\to 0}\sum_m \frac{m^2}{m^2+\varepsilon^2}J_m^2=1-J_0^2(k),\\ &\lim_{\varepsilon\to 0}\sum_m \frac{m^4}{m^2+\varepsilon^2}J_m^2=\sum_m m^2J_m^2(k)=\frac{1}{2}k^2,\\ &\lim_{\varepsilon\to 0}\sum_m \frac{m^6}{m^2+\varepsilon^2}J_m^2=\sum_m m^4J_m^2(k)=2\left(\frac{k}{2}\right)^2\left[1+3\left(\frac{k}{2}\right)^2\right]. \end{aligned}\right\} \tag{A2}$$

3. Asymptotics of products of Bessel functions

$$\left.\begin{aligned} &\lim_{k\to 0}[1-J_0^2(k)]/k^2 = 1/2,\\ &\lim_{k\to 0} 2J_0(k)J_1(k)/k = 1,\\ &\lim_{k\to 0} 2J_0(k)J_2(k)/k^2 = 1/4. \end{aligned}\right\} \tag{A3}$$

Fourier synthesis of infinite series used in the main text

$$\sum_{n=1}^{\infty} \frac{2}{n^2\pi^2+k'^2}\cos n\pi(z+1) = \frac{1}{k'\sinh k'}\left\{\cosh k'z - \frac{\sinh k'}{k'}\right\}, \tag{A4}$$

$$\sum_{n=1}^{\infty} \frac{2n\pi}{(n^2\pi^2+k'^2)^2}\sin n\pi(z+1) = \frac{1}{k'\sinh k'}\left\{z\cosh k'z - \frac{\sinh k'z}{\tanh k'}\right\}, \tag{A5}$$

$$\sum_{n=1}^{\infty} \frac{2}{n\pi}\,\frac{1}{n^2\pi^2+k'^2}\sin n\pi(z+1) = \frac{1}{k'^2\sinh k'}\{\sinh k'z - z\sinh k'. \tag{A6}$$